

Copyright © 2000, by the author(s).
All rights reserved.

Permission to make digital or hard copies of all or part of this work for personal or classroom use is granted without fee provided that copies are not made or distributed for profit or commercial advantage and that copies bear this notice and the full citation on the first page. To copy otherwise, to republish, to post on servers or to redistribute to lists, requires prior specific permission.

**SINGLE-ELECTRON TUNNELING JUNCTION
CELLULAR NONLINEAR NETWORKS**

by

Tao Yang and Leon O. Chua

Memorandum No. UCB/ERL M00/10

9 March 2000

**SINGLE-ELECTRON TUNNELING JUNCTION
CELLULAR NONLINEAR NETWORKS**

by

Tao Yang and Leon O. Chua

Memorandum No. UCB/ERL M00/10

9 March 2000

ELECTRONICS RESEARCH LABORATORY

College of Engineering
University of California, Berkeley
94720

Single-Electron Tunneling Junction Cellular Nonlinear Networks

Tao Yang and Leon O. Chua

Department of Electrical Engineering and Computer Sciences,
University of California at Berkeley,
Berkeley, California, CA 94720, USA

Abstract

In this note we present the circuit model of a single-electron tunneling junction (SETJ) that is driven by a sinusoidal voltage source and biased by a DC voltage source. The model of an isolated SETJ is a first-order non-autonomous *impulsive* differential equation. The tunneling effect of SETJ can be perfectly modeled by the impulsive effect of the junction voltage that is the state variable of our circuit model. We present 1D and 2D SETJ cellular nonlinear network (CNN) arrays to perform Boolean logic operations and cellular operations that can be easily generalized for universal computations. We study the basins of attractions of two periodic solutions, called the two *phase states* of the SETJ, under isolating and coupling conditions. Based on our results, we present a scheme for implementing basic Boolean logic gates based on a 1D SETJ CNN structure, and for implementing *image computation* via a 2D SETJ CNN structure. For convenience of mathematical analysis, we also present the dimensionless form of our circuit models. Some examples are presented to demonstrate the image computation capability of SETJ CNN. In particular, we use a simple 2D SETJ CNN structure to perform both edge and corner detections. Some cellular automata (CA)-like behaviors of our 2D SETJ CNN are also presented.

1 Basic structure and circuit model of isolated SETJ

The main goal of this note is to use a single-electron tunneling junction (SETJ) array to implement cellular operations via the cellular neural network (CNN) paradigm [1, 3, 2]. The block diagram of an isolated SETJ is shown in Fig.1. The small box denotes a SETJ with

junction capacitor C . The voltage across this SETJ is denoted by v_C . Observe that this SETJ is driven by a sinusoidal voltage source

$$v_p(t) = V_p \sin(\omega_p t)$$

and biased by a DC voltage source v_b in series with a resistor R .

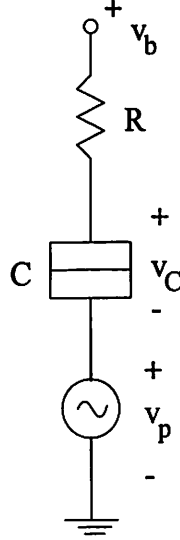


Figure 1: Circuit block diagram of an isolated single-electron tunneling junction.

1.1 Circuit model and its dimensionless form

The dynamics of an isolated SETJ is given by the following non-autonomous impulsive differential equation:

$$\begin{aligned} \frac{dv_C(t)}{dt} &= \frac{1}{RC}(v_b - v_C(t) - V_p \cos(\omega_p t)), & \text{if } v_C(t) < V_T, \\ \Delta v_C(t) &= -2V_T, & \text{if } v_C(t) \geq V_T, \\ & & v_C(0) < V_T. \end{aligned} \tag{1}$$

where $v_C(t)$ is the junction voltage and

$$V_T = \frac{e}{2C}$$

is the *tunneling voltage* and e is the electron charge. By simple algebra we can normalize (1) into the following dimensionless form:

$$\begin{aligned}\frac{d\theta}{ds} &= \gamma \left(a - b \cos s - \frac{\theta}{\pi} \right), & \text{if } \theta < \pi, \\ \Delta\theta &= -2\pi, & \text{if } \theta \geq \pi, \\ & & \theta(0) < \pi.\end{aligned}\tag{2}$$

where

$$a = \frac{v_b}{V_T}, \quad b = \frac{V_p}{V_T}, \quad \theta = \frac{2\pi C v_C}{e}, \quad s = \omega_p t, \quad \gamma = \frac{\pi}{RC\omega_p}.$$

Observe that system (2) is only superficially different from the following representation given in Ref. [4]:

$$\frac{d\theta}{ds} = (a + b \cos s - S(\theta))g\tag{3}$$

where the piecewise linear function $S(\theta)$ is defined by

$$S(\theta) = \frac{\theta}{\pi} - 2n, \quad (2n - 1)\pi \leq \theta < (2n + 1)\pi\tag{4}$$

where n is an integer. Observe also that in model (2), we do not consider the cases when there are more than one electron in the SETJ because we assume that initially the SETJ contains one or less electron. Without loss of generality this assumption will simplify expressions.

1.2 Simulation results of an isolated SETJ cell

To demonstrate that a SETJ cell has two phase states and that our SETJ model in the form of a non-autonomous impulsive differential equation is equivalent to that presented in [4], we numerically solve our SETJ model in Eq. (2) with parameters $a = 1.77$, $b = 2.0$, and $\gamma = 1/3$. The simulation results with two different initial conditions $\theta(0) = -0.2$ and $\theta(0) = 1.8$ are shown in Fig. 2 as solid and dashed curves, respectively. From which we can see that an isolated SETJ can have two stable periodic solutions. Comparing this simulation result with that presented in Fig. 3 of Ref. [4], we can see that they are identical. This verifies that our impulsive differential model is equivalent to that presented in [4]. In Fig. 2, the sudden jumps in the solid and dashed curves occur when electrons tunnel through the SETJ.

Let the pump source signal be a reference signal. The moments of tunneling effects are

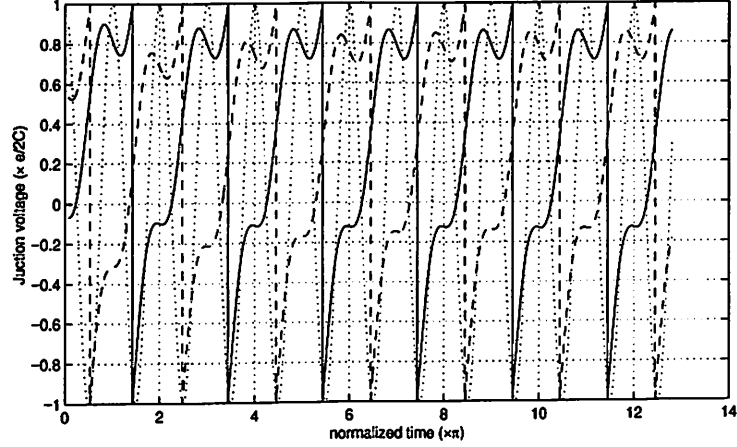


Figure 2: Simulation results of the two phase states generated by an isolated SETJ cell with two different initial conditions.

located approximately at two different phases; namely, at $\pi/2 + 2n\pi$ and $3\pi/2 + 2n\pi$, where n is an integer. However, the exact locations of the tunneling effects will not be exactly at these two phases. As long as the differences between these two phase states are larger than the fluctuation of each phase state, we can still distinguish these two phase states. We will use these two phase states to represent two Boolean logic states.

2 Basic structure and circuit model of two coupled SETJs

Let us consider two SETJs coupled through a capacitor C_{in} in series with a resistor R_{in} as shown in Fig. 3. The dynamics of this circuit model is given by the following non-autonomous

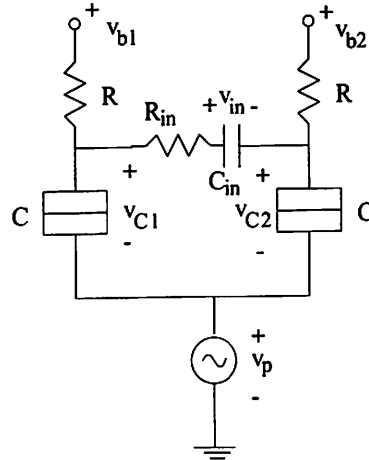


Figure 3: Circuit block diagram of two coupled SETJs.

impulsive differential equations:

$$\begin{aligned}
\frac{dv_{C1}(t)}{dt} &= \frac{1}{RC} \left(v_{b1} - v_{C1}(t) - V_p \cos(\omega_p t) - \frac{v_{C1}(t) - v_{C2}(t) - v_{in}(t)}{k} \right), & \text{if } v_{C1}(t) < V_T, \\
\frac{dv_{C2}(t)}{dt} &= \frac{1}{RC} \left(v_{b2} - v_{C2}(t) - V_p \cos(\omega_p t) + \frac{v_{C1}(t) - v_{C2}(t) - v_{in}(t)}{k} \right), & \text{if } v_{C2}(t) < V_T, \\
\frac{dv_{in}(t)}{dt} &= \frac{1}{RC\epsilon k} (v_{C1}(t) - v_{C2}(t) - v_{in}(t)), \\
\Delta v_{C1}(t) &= -2V_T, & \text{if } v_{C1}(t) \geq V_T, \\
\Delta v_{C2}(t) &= -2V_T, & \text{if } v_{C2}(t) \geq V_T, \\
v_{C1}(0) &< V_T, & v_{C2}(0) < V_T.
\end{aligned} \tag{5}$$

where

$$\epsilon = \frac{C_{in}}{C}, \quad k = \frac{R_{in}}{C}.$$

The dimensionless form is given by

$$\begin{aligned}
\frac{d\theta_1}{ds} &= \gamma \left(a_1 - b \cos s - \frac{(k+1)\theta_1}{k\pi} + \frac{\theta_2}{k\pi} + \frac{\theta_{in}}{k\pi} \right), & \text{if } \theta_1 < \pi, \\
\frac{d\theta_2}{ds} &= \gamma \left(a_2 - b \cos s - \frac{(k+1)\theta_2}{k\pi} + \frac{\theta_1}{k\pi} - \frac{\theta_{in}}{k\pi} \right), & \text{if } \theta_2 < \pi, \\
\frac{d\theta_{in}}{ds} &= \frac{\gamma}{k\epsilon\pi} (\theta_1 - \theta_2 - \theta_{in}), \\
\Delta\theta_1 &= -2\pi, & \text{if } \theta_1 \geq \pi, \\
\Delta\theta_2 &= -2\pi, & \text{if } \theta_2 \geq \pi, \\
\theta_1(0) &< \pi, & \theta_2(0) < \pi.
\end{aligned} \tag{6}$$

where

$$a_1 = \frac{v_{b1}}{V_T}, \quad \theta_1 = \frac{2\pi C v_{C1}}{e}, \quad a_2 = \frac{v_{b2}}{V_T}, \quad \theta_2 = \frac{2\pi C v_{C2}}{e}, \quad \theta_{in} = \frac{2\pi C v_{in}}{e}.$$

2.1 Simulation results of two coupled SETJs

The simulation results of the two coupled SETJs are shown in Fig. 4. In this simulation, the parameters are chosen as $a_1 = a_2 = 2$, $b = 2$, $\gamma = 1/3$, $\epsilon = 0.5$, and $k = 0.1$. The initial conditions are chosen as $\theta_1(0) = 0.2$, $\theta_2(0) = 0.0$, and $\theta_{in}(0) = 0.0$. The waveform of $\theta_1(t)$, $\theta_2(t)$, and $\theta_{in}(t)$ are shown in solid, dashed and dash-dotted curves, respectively. Comparing the result shown in Fig.9 in Ref. [4] with that shown in Fig. 4(a), we can see that the final results of these two simulations are the same even though the transient processes at the beginning are different because different $\theta_{in}(0)$ s were used. Figure 4(b) shows the distribution

of the two phase states in SETJs 1 and 2 after the transient process dies out. Observe that the two phase states are not exactly at $\pi/2$ and $3\pi/2$. However, the performance of this two coupled SETJs are still robust enough to distinguish these two phase states.

To show that the parameter v_b can easily change the behavior of the coupled SETJs, we change a_1 to 1 and keep all other parameters unchanged. The simulation results are shown in Fig. 4(c) and (d). Observe that in this case, both SETJs can stay at two different phase states. And the locations of each phase state had spread into a small region instead of a single point. Since Fig. 4(b) and (d) are in fact the Pointcaré maps of the two coupled SETJ model, when the locations of phase states are spread out, it means that the trajectories may belong to a multi-periodic or even chaotic attractor. However, the histogram shows that even in this case, the two phase states can be easily distinguished. This provides us with a method of controlling the behaviors of SETJs by using different biases. Of course, another parameter, V_p , can also be used as the second controlling parameter.

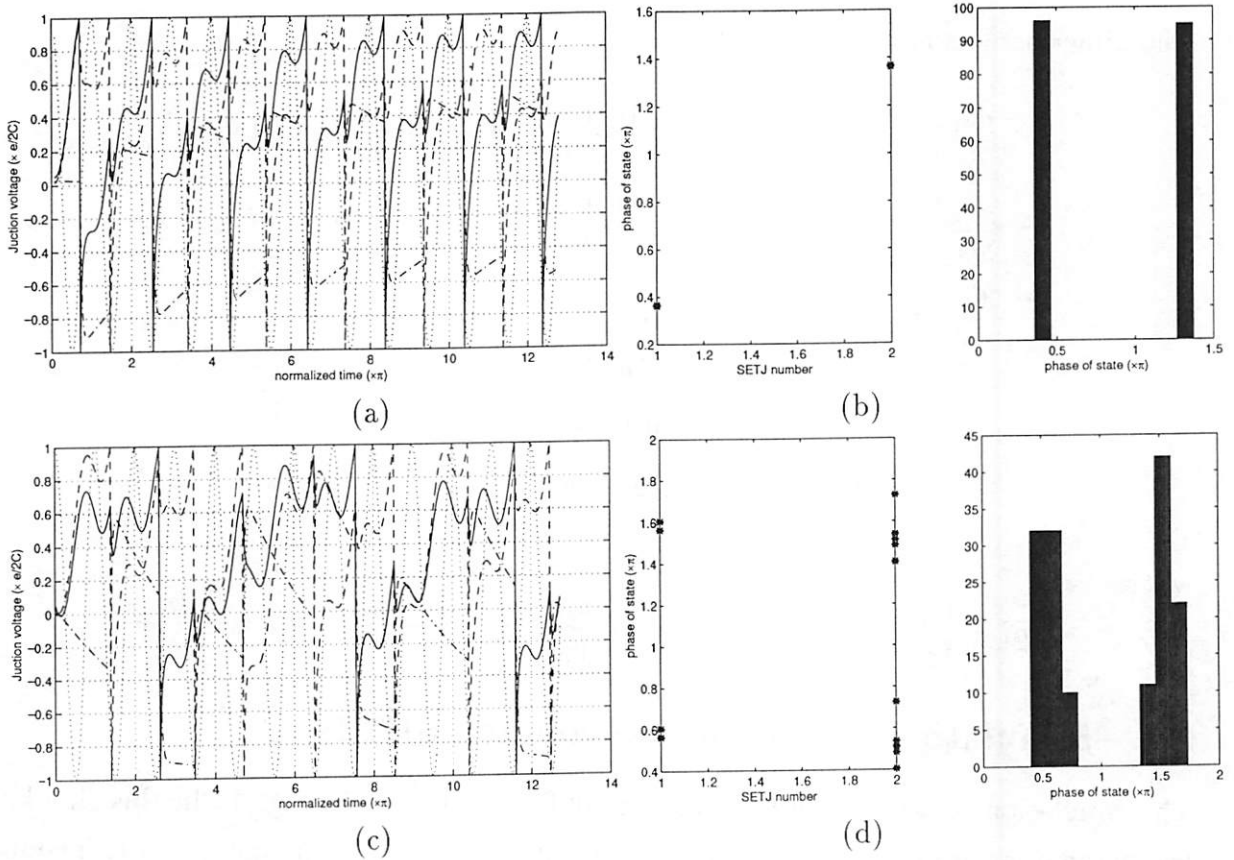


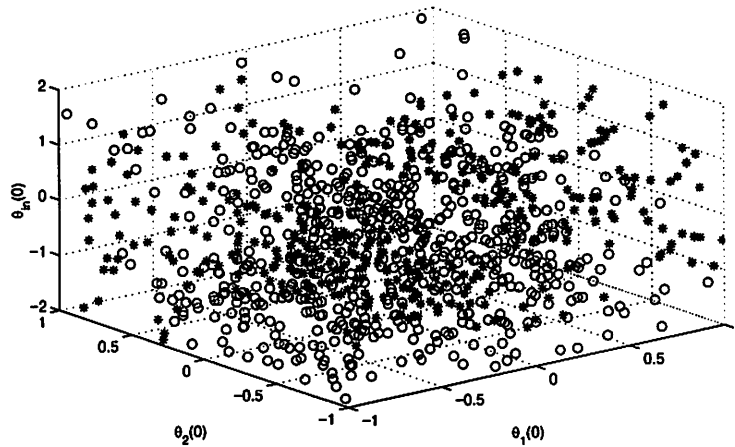
Figure 4: Simulation results of two coupled SETJs. (a) The phase states of two SETJs are stable when $a_1 = a_2 = 2$. (b) The histogram of the two phase states corresponding to (a). (c) The phase states of the two SETJs are no longer stable when we change a_1 to 1 while other conditions are kept unchanged. (d) The histogram of the two phase states corresponding to (c).

2.2 Equalizing and NOTing logic operations

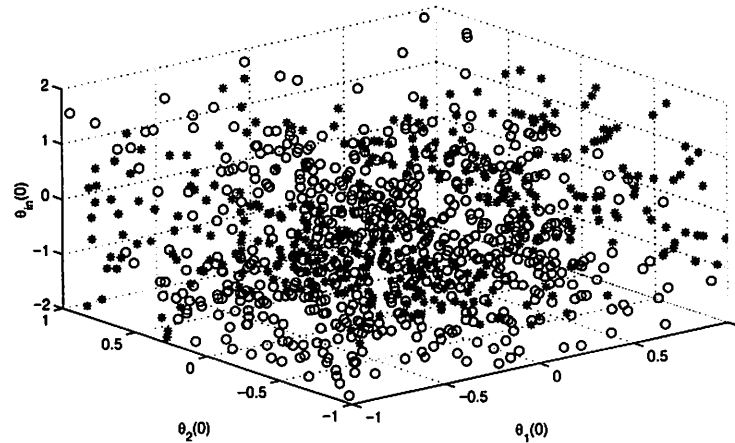
We will now present examples to show that by choosing different values for v_d , the two coupled SETJs can perform different Boolean logic operations regardless of initial conditions. In the following simulations the fixed parameters are given by $b = 2$, $\gamma = 1/3$, $\epsilon = 0.5$, and $k = 0.1$. To show that our results are independent of initial conditions, we randomly choose $\theta_1(0) \in (-\pi, \pi)$, $\theta_2(0) \in (-\pi, \pi)$, and $\theta_{in}(0) \in (-2\pi, 2\pi)$ in our simulations.

2.2.1 Case 1: $a_1 = a_2 = 1$

The simulation results are shown in Fig. 5. Observe that in this case, the output of both SETJs are equal regardless of initial conditions.



(a)



(b)

Figure 5: The stable phase states of two coupled SETJs under different initial conditions. The symbols “*” and “o” denote logic TRUTH and logic FALSE, respectively. (a) SETJ 1. (b) SETJ 2.

2.2.2 Case 2: $a_1 = a_2 = 2$

The simulation results are shown in Fig. 6. Observe that in this case, the output of both SETJs are inverse of each other regardless of initial conditions.

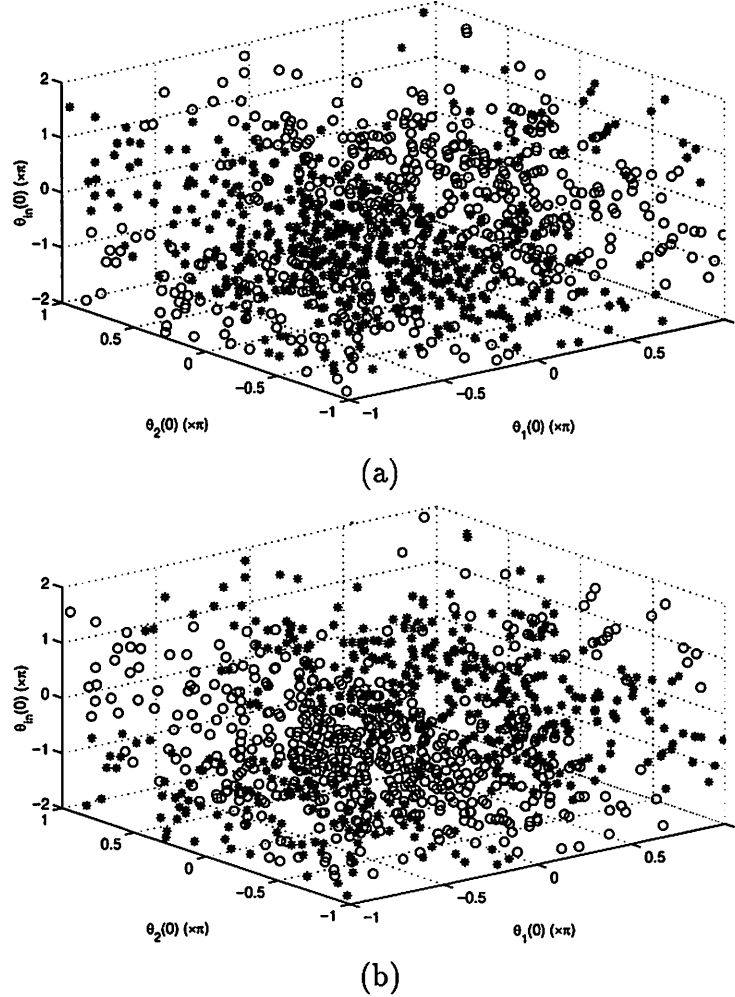


Figure 6: The stable phase states of two coupled SETJs under different initial conditions. The symbols “*” and “o” denote logic TRUTH and logic FALSE, respectively. (a) SETJ 1. (b) SETJ 2.

The phenomena shown in the Figs. 5 and 6 can have many applications. For example, a robust and reliable memory unit can be built if we use the equal state and NOTing state to denote two logic values. The initial condition insensitivity can be used to build very reliable memory units that can store digital bits regardless of its original states. This is a much better choice than using a single SETJ as a basic memory unit whose memorized state is sensitive to initial conditions. That the initial states of SETJs are most likely inaccessible make the initial-state independent scheme the best way to design memory units.

2.2.3 Case 3: $a_1 = 1$ and $a_2 = 2$

The simulation results are shown in Fig. 7. Observe that in this case, the outputs of both SETJs can visit two phase states regardless of initial conditions.¹

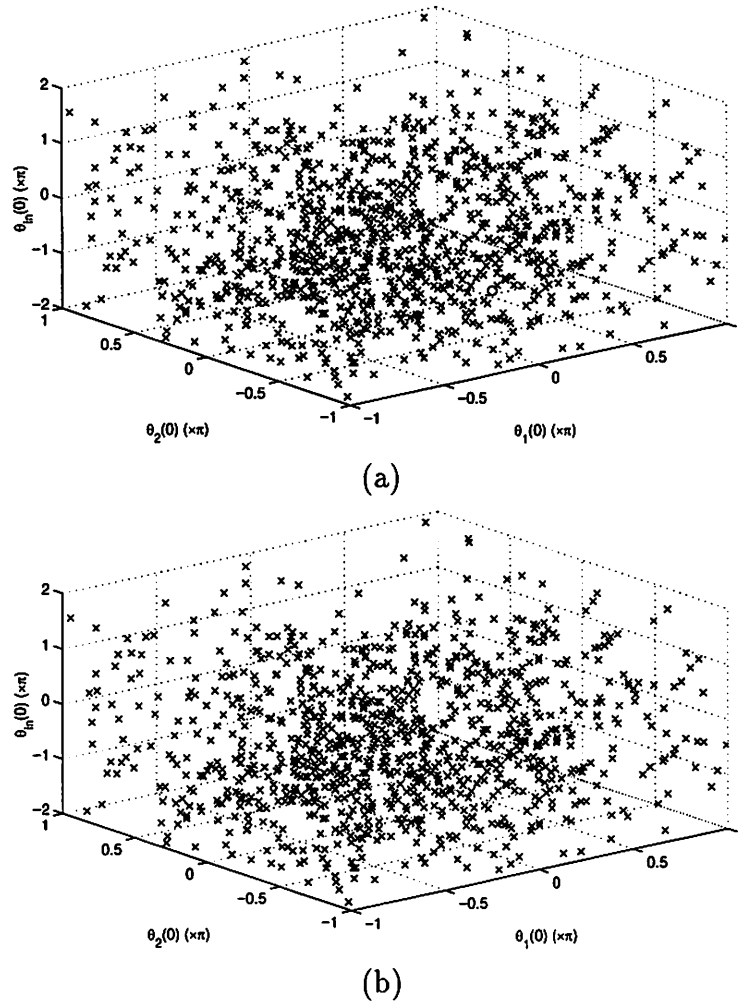


Figure 7: The stable phase states of two coupled SETJs under different initial conditions. The symbols “*” and “o” denote logic TRUTH and logic FALSE, respectively. The symbol “x” denotes that a SETJ can show both logic TRUTH and logic FALSE in its evolution. (a) SETJ 1. (b) SETJ 2.

3 Basic structure and circuit model of three coupled SETJs

¹In fact, in 1000 sets of initial conditions, only one set violates this conclusion.

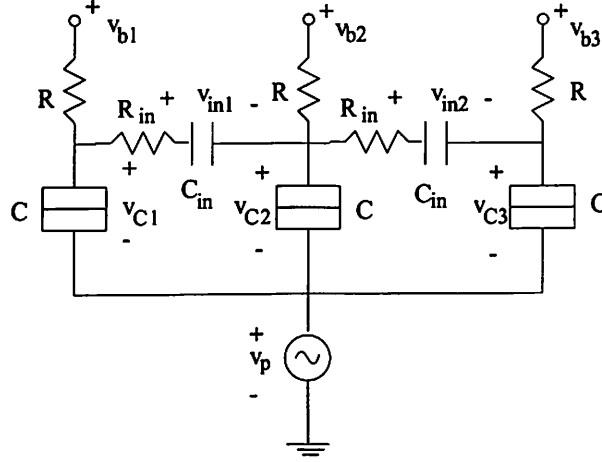


Figure 8: Block diagram of three coupled SETJs.

Let us consider next three SETJs coupled through capacitors C_{in} in series with resistors R_{in} as shown in Fig. 8. Let us assume that $C_{in1} = C_{in2} = C_{in}$. The dynamics of the circuit model is given by the following non-autonomous impulsive differential equations:

$$\begin{aligned}
\frac{dv_{C1}(t)}{dt} &= \frac{1}{RC} \left(v_{b1} - v_{C1}(t) - V_p \cos(\omega_p t) - \frac{v_{C1}(t) - v_{C2}(t) - v_{in1}(t)}{k} \right), \quad \text{if } v_{C1}(t) < V_T, \\
\frac{dv_{C2}(t)}{dt} &= \frac{1}{RC} \left(v_{b2} - v_{C2}(t) - V_p \cos(\omega_p t) + \frac{v_{C1}(t) - v_{C2}(t) - v_{in1}(t)}{k} \right. \\
&\quad \left. - \frac{v_{C2}(t) - v_{C3}(t) - v_{in2}(t)}{k} \right), \quad \text{if } v_{C2}(t) < V_T, \\
\frac{dv_{C3}(t)}{dt} &= \frac{1}{RC} \left(v_{b3} - v_{C3}(t) - V_p \cos(\omega_p t) + \frac{v_{C2}(t) - v_{C3}(t) - v_{in2}(t)}{k} \right), \quad \text{if } v_{C3}(t) < V_T, \\
\frac{dv_{in1}(t)}{dt} &= \frac{1}{RC\epsilon k} (v_{C1}(t) - v_{C2}(t) - v_{in1}(t)), \\
\frac{dv_{in2}(t)}{dt} &= \frac{1}{RC\epsilon k} (v_{C2}(t) - v_{C3}(t) - v_{in2}(t)), \\
\Delta v_{C1}(t) &= -2V_T, \quad \text{if } v_{C1}(t) \geq V_T, \\
\Delta v_{C2}(t) &= -2V_T, \quad \text{if } v_{C2}(t) \geq V_T, \\
\Delta v_{C3}(t) &= -2V_T, \quad \text{if } v_{C3}(t) \geq V_T, \\
v_{C1}(0) &< V_T, \quad v_{C2}(0) < V_T, \quad v_{C3}(0) < V_T.
\end{aligned} \tag{7}$$

The dimensionless form is given by the following non-autonomous impulsive differential equations:

$$\frac{d\theta_1}{ds} = \gamma \left(a_1 - b \cos s - \frac{(k+1)\theta_1}{k\pi} + \frac{\theta_2}{k\pi} + \frac{\theta_{in1}}{k\pi} \right), \quad \text{if } \theta_1 < \pi,$$

$$\begin{aligned}
\frac{d\theta_2}{ds} &= \gamma \left(a_2 - b \cos s - \frac{(k+2)\theta_2}{k\pi} + \frac{\theta_1}{k\pi} + \frac{\theta_3}{k\pi} - \frac{\theta_{in1}}{k\pi} + \frac{\theta_{in2}}{k\pi} \right), \quad \text{if } \theta_2 < \pi, \\
\frac{d\theta_3}{ds} &= \gamma \left(a_3 - b \cos s - \frac{(k+1)\theta_3}{k\pi} + \frac{\theta_2}{k\pi} - \frac{\theta_{in2}}{k\pi} \right), \quad \text{if } \theta_3 < \pi, \\
\frac{d\theta_{in1}}{ds} &= \frac{\gamma}{k\epsilon\pi} (\theta_1 - \theta_2 - \theta_{in1}), \\
\frac{d\theta_{in2}}{ds} &= \frac{\gamma}{k\epsilon\pi} (\theta_2 - \theta_3 - \theta_{in2}), \\
\Delta\theta_1 &= -2\pi, \quad \text{if } \theta_1 \geq \pi, \\
\Delta\theta_2 &= -2\pi, \quad \text{if } \theta_2 \geq \pi, \\
\Delta\theta_3 &= -2\pi, \quad \text{if } \theta_3 \geq \pi, \\
\theta_1(0) &< \pi, \quad \theta_2(0) < \pi, \quad \theta_3(0) < \pi.
\end{aligned} \tag{8}$$

where

$$a_3 = \frac{v_{b3}}{V_T}, \quad \theta_3 = \frac{2\pi C v_{C3}}{e}, \quad \theta_{in1} = \frac{2\pi C v_{in1}}{e}, \quad \theta_{in2} = \frac{2\pi C v_{in2}}{e}.$$

3.1 Simulation results

In this section, we show simulation results of three coupled SETJs. The fixed parameters are given by: $b = 2$, $\gamma = 1/3$, and $k = 0.1$. We randomly choose $\theta_1(0) \in (-\pi, \pi)$, $\theta_2(0) \in (-\pi, \pi)$, $\theta_3(0) \in (-\pi, \pi)$, $\theta_{in1}(0) \in (-2\pi, 2\pi)$ and $\theta_{in2}(0) \in (-2\pi, 2\pi)$ in our simulations.

3.1.1 $a_1 = a_2 = a_3 = 2$, $\epsilon = 0.5$

Under most initial conditions, the three coupled SETJs implement the following truth table, where Ψ_1 , Ψ_2 , and Ψ_3 denote the truth value of the three SETJ cells, respectively. This truth table can be verified by results shown in Fig. 9.

Table 1: Truth table for three coupled SETJs with $a_1 = a_2 = a_3 = 2$ and $\epsilon = 0.5$.

Ψ_1	Ψ_2	Ψ_3
FALSE	TRUE	FALSE
TRUE	FALSE	TRUE

3.1.2 $a_1 = a_2 = a_3 = 2$, $\epsilon = 1$

In this case, the three coupled SETJs implement the following truth table:

Table 2: Truth table for three coupled SETJs with $a_1 = a_2 = a_3 = 2$ and $\epsilon = 1$.

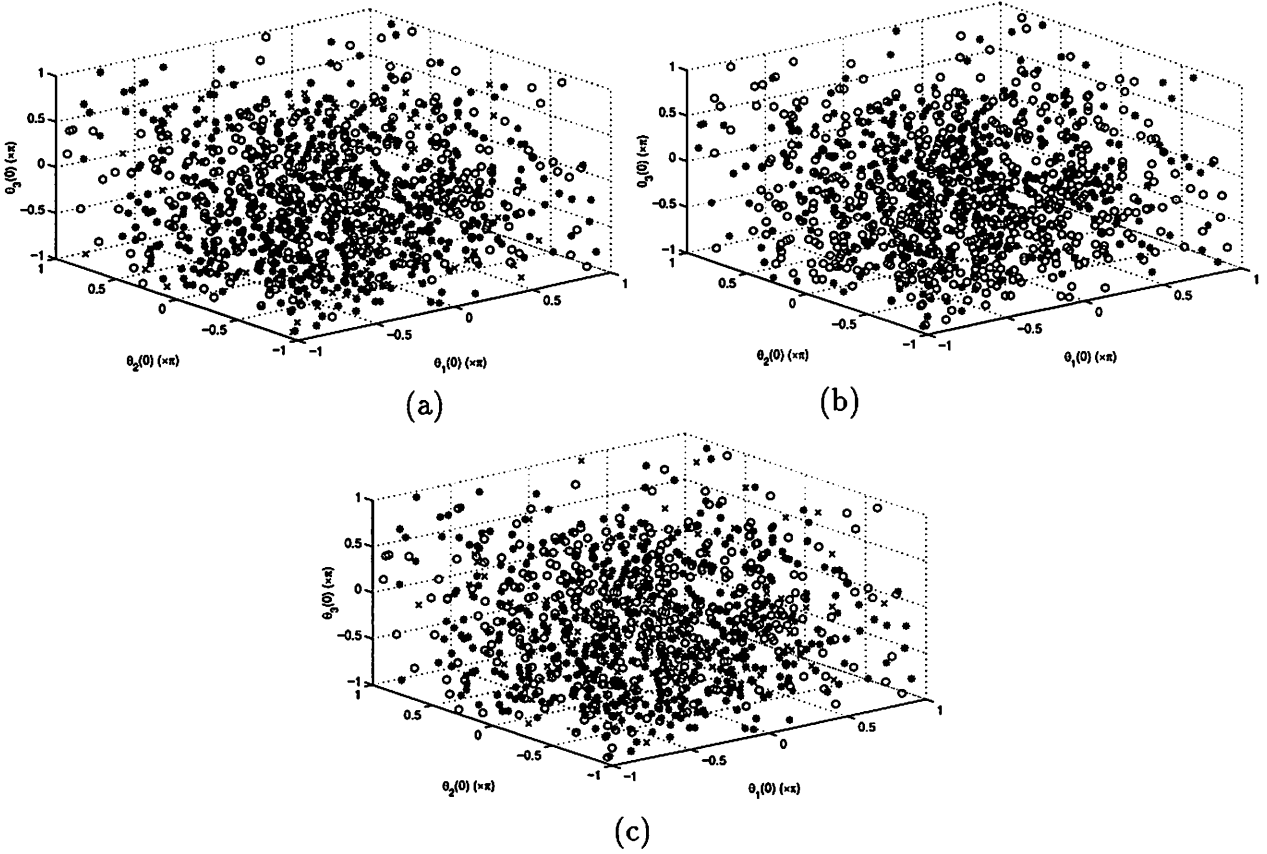


Figure 9: The stable phase states of three coupled SETJs under different initial conditions. The symbols “*” and “o” denote logic TRUTH and logic FALSE, respectively. The symbol “×” denotes that the SETJ can show both logic TRUTH and logic FALSE in its revolution. (a) SETJ 1. (b) SETJ 2. (c) SETJ 3.

Ψ_1	Ψ_2	Ψ_3
0	0	1
0	1	0
0	1	1
1	0	0
1	0	1
1	1	0

Observe that this truth table excludes the possibility of $(\Psi_1, \Psi_2, \Psi_3) = (0, 0, 0)$ and $(\Psi_1, \Psi_2, \Psi_3) = (1, 1, 1)$. Since the parameter space and the behaviors of non-autonomous impulsive differential equation can be very complex, there may be many different truth tables that can be implemented by three coupled SETJs.

4 One-dimensional SETJ CNN

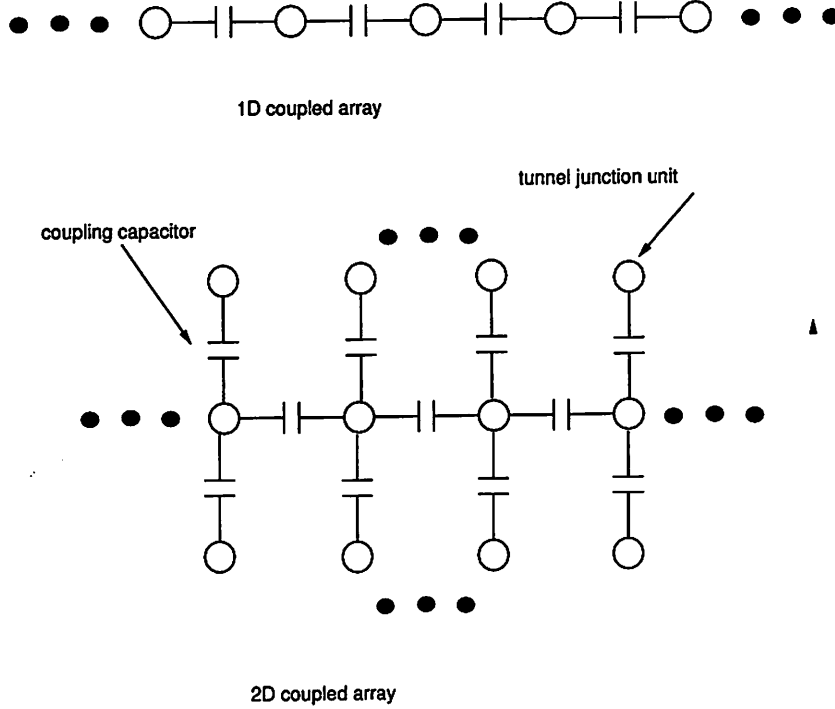


Figure 10: Coupling single-electron junctions into 1D or 2D CNN arrays.

Unlike a standard CNN array, in a SETJ CNN, the boundary cells has to be clearly defined. In this section, we set up the model of a 1D SETJ CNN as shown in the upper part of Fig. 10. Suppose that there are n cells in a 1D SETJ CNN array. Then the first and the n th cell are the left and the right boundary cells. For three coupled SETJs, the left and the right SETJs can be viewed as the left and right boundary cells, respectively. Similarly, the center cell in a three coupled SETJs represents an example of an inner cell in a 1D SETJ CNN. By slightly modifying the results in Sec. 3, we get the following dimensionless form of a 1D SETJ CNN with $n \geq 3$ cells:

$$\begin{aligned} \frac{d\theta_1}{ds} &= \gamma \left(a_1 - b \cos s - \frac{(k+1)\theta_1}{k\pi} + \frac{\theta_2}{k\pi} + \frac{\vartheta_1}{k\pi} \right), \quad \text{if } \theta_1 < \pi, \\ \frac{d\theta_2}{ds} &= \gamma \left(a_2 - b \cos s - \frac{(k+2)\theta_2}{k\pi} + \frac{\theta_1}{k\pi} + \frac{\theta_3}{k\pi} - \frac{\vartheta_1}{k\pi} + \frac{\vartheta_2}{k\pi} \right), \quad \text{if } \theta_2 < \pi, \end{aligned}$$

$$\begin{aligned}
& \vdots \\
\frac{d\theta_i}{ds} &= \gamma \left(a_i - b \cos s - \frac{(k+2)\theta_i}{k\pi} + \frac{\theta_{i-1}}{k\pi} + \frac{\theta_{i+1}}{k\pi} - \frac{\vartheta_{i-1}}{k\pi} + \frac{\vartheta_i}{k\pi} \right), \quad \text{if } \theta_i < \pi, \\
& \vdots \\
\frac{d\theta_n}{ds} &= \gamma \left(a_n - b \cos s - \frac{(k+1)\theta_n}{k\pi} + \frac{\theta_{n-1}}{k\pi} - \frac{\vartheta_{n-1}}{k\pi} \right), \quad \text{if } \theta_n < \pi, \\
\frac{d\vartheta_1}{ds} &= \frac{\gamma}{k\epsilon\pi} (\theta_1 - \theta_2 - \vartheta_1), \\
& \vdots \\
\frac{d\vartheta_i}{ds} &= \frac{\gamma}{k\epsilon\pi} (\theta_i - \theta_{i+1} - \vartheta_i), \\
& \vdots \\
\frac{d\vartheta_{n-1}}{ds} &= \frac{\gamma}{k\epsilon\pi} (\theta_{n-1} - \theta_n - \vartheta_{n-1}), \\
& \Delta\theta_i = -2\pi, \quad \text{if } \theta_i \geq \pi, \quad i = 1, 2, \dots, n-1, n, \\
& \theta_i(0) < \pi, \quad i = 1, 2, \dots, n-1, n.
\end{aligned} \tag{9}$$

where θ_i denotes the state variables of the i th SETJ and ϑ_i denotes the state variables of the coupling capacitor between the i th and the $(i+1)$ th SETJs.

5 Two-dimensional SETJ CNN

In this section we consider a 2D SETJ CNN with a 4-connected (von Neumann) neighborhood system, as shown in the lower part of Fig. 10. This class of CNN can be modeled by the following non-autonomous impulsive differential equations. Let us suppose that the CNN array consists of $M \times N$ SETJ cells, then an inner cells C_{ij} , $1 < i < M$, $1 < j < N$, is given by

$$\begin{aligned}
\frac{dx_{ij}}{dt} &= \gamma \left(u_{ij} - b \cos t - \frac{(k+4)x_{ij}}{k\pi} + \frac{x_{i,j-1}}{k\pi} + \frac{x_{i,j+1}}{k\pi} + \frac{x_{i-1,j}}{k\pi} + \frac{x_{i+1,j}}{k\pi} \right. \\
&\quad \left. - \frac{q_{ij}}{k\pi} + \frac{q_{i,j+1}}{k\pi} - \frac{p_{ij}}{k\pi} + \frac{p_{i+1,j}}{k\pi} \right), \quad \text{if } x_{ij} < \pi, \\
\frac{dp_{ij}}{dt} &= \frac{\gamma}{k\epsilon\pi} (x_{i-1,j} - x_{ij} - p_{ij}), \\
\frac{dq_{ij}}{dt} &= \frac{\gamma}{k\epsilon\pi} (x_{i,j-1} - x_{ij} - q_{ij}),
\end{aligned}$$

$$\Delta x_{ij} = -2\pi, \quad \text{if } x_{ij} \geq \pi,$$

$$x_{ij}(0) < \pi, \quad 1 < i < M, \quad 1 < j < N, \quad (10)$$

where x_{ij} is the state variable of the SETJ at location (i, j) . p_{ij} is the state variable modeling the capacitive coupling between cell $C_{i-1,j}$ and C_{ij} . q_{ij} is the state variable modeling the capacitive coupling between cell $C_{i,j-1}$ and C_{ij} . Since in a SETJ CNN array, boundary conditions play very important roles in the dynamics of the entire array, we should define the boundary condition explicitly. We define the boundary cells in the first and the last columns as follows:

$$\begin{aligned} \frac{dx_{ij}}{dt} &= \gamma \left(u_{ij} - b \cos t - \frac{(k+3)x_{ij}}{k\pi} + \frac{x_{i,j+1}}{k\pi} + \frac{x_{i-1,j}}{k\pi} + \frac{x_{i+1,j}}{k\pi} \right. \\ &\quad \left. + \frac{q_{i,j+1}}{k\pi} - \frac{p_{ij}}{k\pi} + \frac{p_{i+1,j}}{k\pi} \right), \quad \text{if } x_{ij} < \pi, \\ \frac{dp_{ij}}{dt} &= \frac{\gamma}{k\epsilon\pi} (x_{i-1,j} - x_{ij} - p_{ij}), \\ \Delta x_{ij} &= -2\pi, \quad \text{if } x_{ij} \geq \pi, \\ x_{ij}(0) &< \pi, \quad 1 < i < M, \quad j = 1. \end{aligned} \quad (11)$$

and

$$\begin{aligned} \frac{dx_{ij}}{dt} &= \gamma \left(u_{ij} - b \cos t - \frac{(k+3)x_{ij}}{k\pi} + \frac{x_{i,j-1}}{k\pi} + \frac{x_{i-1,j}}{k\pi} + \frac{x_{i+1,j}}{k\pi} \right. \\ &\quad \left. - \frac{q_{ij}}{k\pi} - \frac{p_{ij}}{k\pi} + \frac{p_{i+1,j}}{k\pi} \right), \quad \text{if } x_{ij} < \pi, \\ \frac{dp_{ij}}{dt} &= \frac{\gamma}{k\epsilon\pi} (x_{i-1,j} - x_{ij} - p_{ij}), \\ \frac{dq_{ij}}{dt} &= \frac{\gamma}{k\epsilon\pi} (x_{i,j-1} - x_{ij} - q_{ij}), \\ \Delta x_{ij} &= -2\pi, \quad \text{if } x_{ij} \geq \pi, \\ x_{ij}(0) &< \pi, \quad 1 < i < M, \quad j = N. \end{aligned} \quad (12)$$

We define the boundary cells in the first and the last rows as follows:

$$\begin{aligned} \frac{dx_{ij}}{dt} &= \gamma \left(u_{ij} - b \cos t - \frac{(k+3)x_{ij}}{k\pi} + \frac{x_{i,j-1}}{k\pi} + \frac{x_{i,j+1}}{k\pi} + \frac{x_{i+1,j}}{k\pi} \right. \\ &\quad \left. - \frac{q_{ij}}{k\pi} + \frac{q_{i,j+1}}{k\pi} + \frac{p_{i+1,j}}{k\pi} \right), \quad \text{if } x_{ij} < \pi, \\ \frac{dq_{ij}}{dt} &= \frac{\gamma}{k\epsilon\pi} (x_{i,j-1} - x_{ij} - q_{ij}), \end{aligned}$$

$$\begin{aligned}\Delta x_{ij} &= -2\pi, \quad \text{if } x_{ij} \geq \pi, \\ x_{ij}(0) &< \pi, \quad 1 < j < N, \quad i = 1.\end{aligned}\tag{13}$$

and

$$\begin{aligned}\frac{dx_{ij}}{dt} &= \gamma \left(u_{ij} - b \cos t - \frac{(k+3)x_{ij}}{k\pi} + \frac{x_{i,j-1}}{k\pi} + \frac{x_{i,j+1}}{k\pi} + \frac{x_{i-1,j}}{k\pi} \right. \\ &\quad \left. - \frac{q_{ij}}{k\pi} + \frac{q_{i,j+1}}{k\pi} - \frac{p_{ij}}{k\pi} \right), \quad \text{if } x_{ij} < \pi, \\ \frac{dp_{ij}}{dt} &= \frac{\gamma}{k\epsilon\pi} (x_{i-1,j} - x_{ij} - p_{ij}), \\ \frac{dq_{ij}}{dt} &= \frac{\gamma}{k\epsilon\pi} (x_{i,j-1} - x_{ij} - q_{ij}), \\ \Delta x_{ij} &= -2\pi, \quad \text{if } x_{ij} \geq \pi, \\ x_{ij}(0) &< \pi, \quad 1 < j < N, \quad i = M.\end{aligned}\tag{14}$$

We define 4 corner cells as follows:

$$\begin{aligned}\frac{dx_{ij}}{dt} &= \gamma \left(u_{ij} - b \cos t - \frac{(k+2)x_{ij}}{k\pi} + \frac{x_{i,j+1}}{k\pi} + \frac{x_{i+1,j}}{k\pi} \right. \\ &\quad \left. + \frac{q_{i,j+1}}{k\pi} + \frac{p_{i+1,j}}{k\pi} \right), \quad \text{if } x_{ij} < \pi, \\ \Delta x_{ij} &= -2\pi, \quad \text{if } x_{ij} \geq \pi, \\ x_{ij}(0) &< \pi, \quad i = 1, \quad j = 1.\end{aligned}\tag{15}$$

$$\begin{aligned}\frac{dx_{ij}}{dt} &= \gamma \left(u_{ij} - b \cos t - \frac{(k+2)x_{ij}}{k\pi} + \frac{x_{i,j-1}}{k\pi} + \frac{x_{i+1,j}}{k\pi} \right. \\ &\quad \left. - \frac{q_{ij}}{k\pi} + \frac{p_{i+1,j}}{k\pi} \right), \quad \text{if } x_{ij} < \pi, \\ \frac{dq_{ij}}{dt} &= \frac{\gamma}{k\epsilon\pi} (x_{i,j-1} - x_{ij} - q_{ij}), \\ \Delta x_{ij} &= -2\pi, \quad \text{if } x_{ij} \geq \pi, \\ x_{ij}(0) &< \pi, \quad i = 1, \quad j = N.\end{aligned}\tag{16}$$

$$\begin{aligned}\frac{dx_{ij}}{dt} &= \gamma \left(u_{ij} - b \cos t - \frac{(k+2)x_{ij}}{k\pi} + \frac{x_{i,j+1}}{k\pi} + \frac{x_{i-1,j}}{k\pi} \right. \\ &\quad \left. + \frac{q_{i,j+1}}{k\pi} - \frac{p_{ij}}{k\pi} \right), \quad \text{if } x_{ij} < \pi,\end{aligned}$$

$$\begin{aligned}
\frac{dp_{ij}}{dt} &= \frac{\gamma}{k\epsilon\pi}(x_{i-1,j} - x_{ij} - p_{ij}), \\
\Delta x_{ij} &= -2\pi, \quad \text{if } x_{ij} \geq \pi, \\
x_{ij}(0) &< \pi, \quad i = M, \quad j = 1.
\end{aligned} \tag{17}$$

$$\begin{aligned}
\frac{dx_{ij}}{dt} &= \gamma \left(u_{ij} - b \cos t - \frac{(k+2)x_{ij}}{k\pi} + \frac{x_{i,j-1}}{k\pi} + \frac{x_{i-1,j}}{k\pi} \right. \\
&\quad \left. - \frac{q_{ij}}{k\pi} - \frac{p_{ij}}{k\pi} \right), \quad \text{if } x_{ij} < \pi, \\
\frac{dp_{ij}}{dt} &= \frac{\gamma}{k\epsilon\pi}(x_{i-1,j} - x_{ij} - p_{ij}), \\
\frac{dq_{ij}}{dt} &= \frac{\gamma}{k\epsilon\pi}(x_{i,j-1} - x_{ij} - q_{ij}), \\
\Delta x_{ij} &= -2\pi, \quad \text{if } x_{ij} \geq \pi, \\
x_{ij}(0) &< \pi, \quad i = M, \quad j = N.
\end{aligned} \tag{18}$$

Observe that the DC biases in the isolated SETJs are now replaced by the *input image array* $\{u_{ij}\}$. Unlike standard CMOS CNN structures where the coupling weights are programmable, in a SETJ CNN, coupling capacitors are physically fabricated and thus may be very difficult to change. In this case, the cellular operations that defined by local rules have to be implemented through adaptable items such as the DC bias of each SETJ cell and the pump voltage source for the entire SETJ CNN array.

5.1 SETJ edge and corner detection

In the standard CNN, corner detection and edge detection can be implemented by two fundamental CNNs[1]. In this section we show that the edge and corner detection can be performed by a single SETJ CNN operation. The simulation results are shown in Fig. 11. Figure 11(a) shows the binary input image $\{u_{ij}\}$, which functions as DC biases for the SETJ CNN array. The DC biases in black and white regions are set as 1 and 2, respectively. Figure 11(b) shows the phase states of cells in the array at $t = 23$ time units. The black, gray and white regions have phase states -1 , 0 , and 1 , respectively. Here, 0 and 1 correspond to $\pi/2$ and $3\pi/2$ phases, respectively. -1 corresponds to a SETJ cell that oscillates between phases $\pi/2$ and $3\pi/2$.

Observe that the black regions show the inner and outer boundaries of the objects and also mark the four corners by four black crosses. Figure 11(c) shows the phase states of cells in the array at $t = 100$ time units. Observe that the typical characteristics of cellular

automata (CA) are displayed in this image. Figure 11(d) shows the phase states of cells in the array at $t = 200$ time units. Observe that the characteristics of CA are also displayed in this image.

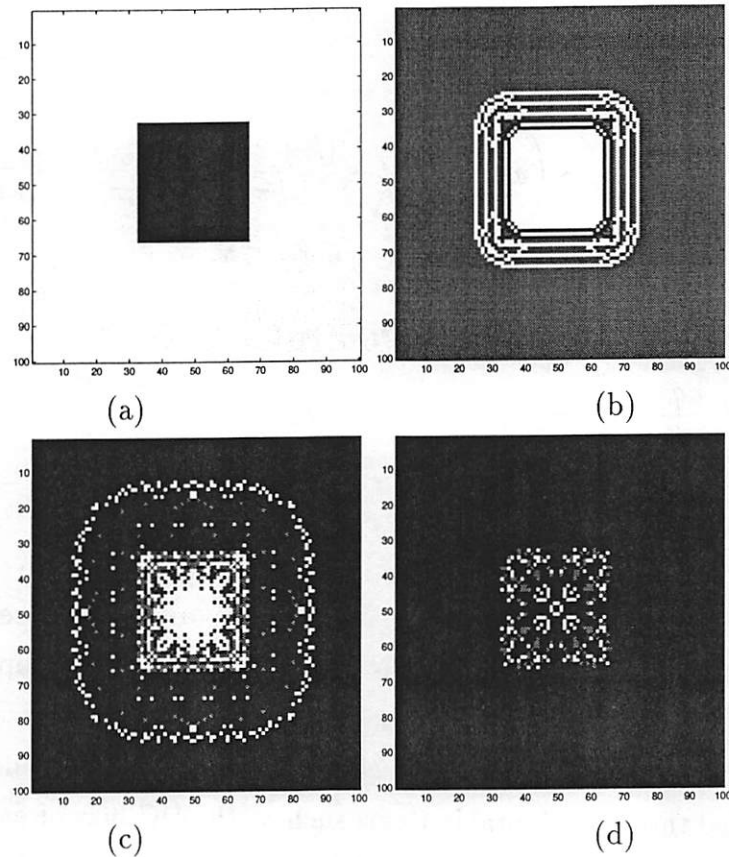


Figure 11: Simulation result of corner and edge detection performed by a SETJ CNN. Parameters are given by: $b = 2$, $\gamma = 1/3$, $\epsilon = 1$, and $k = 0.1$. The fixed simulation step is 0.1. The initial conditions are: $x_{ij}(0) = u_{ij}$, $p_{ij}(0) = q_{ij}(0) = 0$. (a) The input image u_{ij} . (b) The phase state at $t = 23$ time units shows boundaries and corners. (c) The phase state at $t = 100$ time units shows some characteristics of a 2D CA. (d) The phase state at $t = 200$ time units shows some characteristics of a 2D CA.

In the next simulation, only the color of the input image is changed while all other conditions are kept unchanged. The simulation results are shown in Fig. 12. Figure 12(a) shows the input image. Figure 12(b) shows the phase state at $t = 30$ time units. Observe that the boundaries, corners and even the center of the white object are displayed. Figure 12(c) shows the phase state at $t = 200$ time units. Observe that the center of the white object is shown.

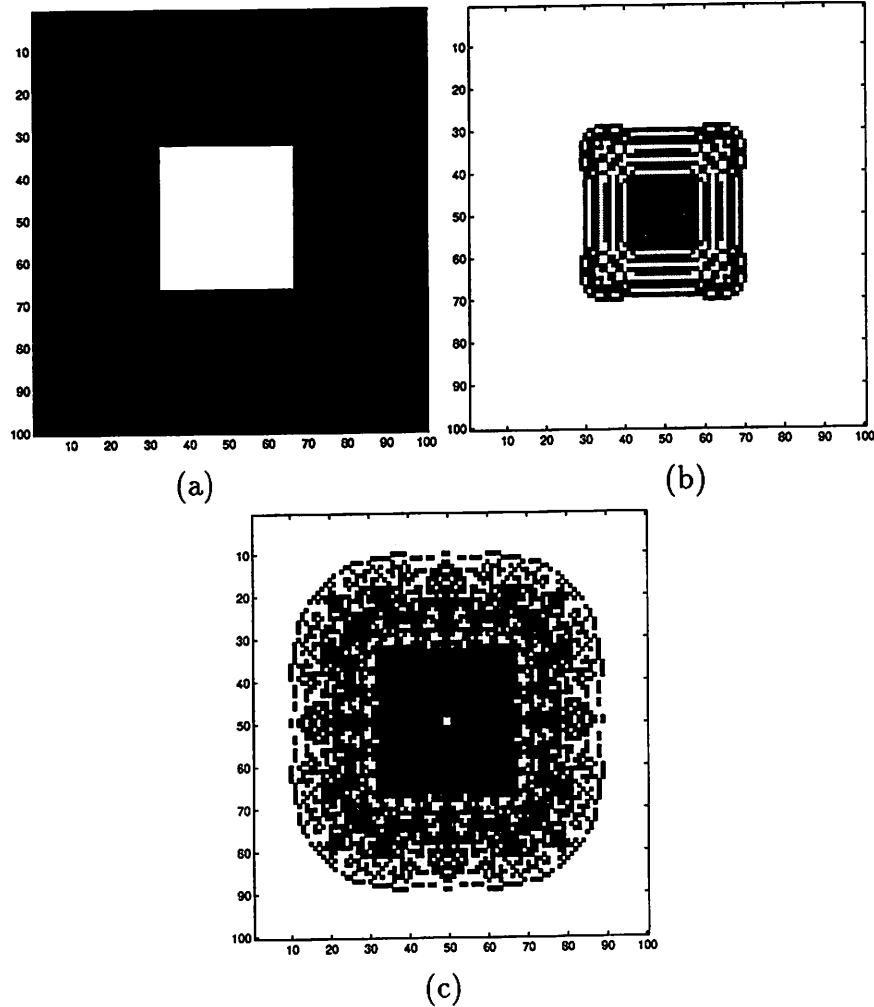


Figure 12: Simulation result of corner and edge detection performed by a SETJ CNN. Parameters are given by: $b = 2$, $\gamma = 1/3$, $\epsilon = 1$, and $k = 0.1$. The fixed simulation step is 0.1. The initial conditions are: $x_{ij}(0) = u_{ij}$, $p_{ij}(0) = q_{ij}(0) = 0$. (a) The input image u_{ij} . (b) The phase state at $t = 30$ time units shows the boundaries, corners and center. (c) The phase state at $t = 200$ time units shows some characteristics of a 2D CA.

6 Concluding remarks

Although in this note we only present some simple examples of applications of 1D and 2D SETJ CNNs to Boolean logic and cellular operations, the extremely complex behaviors of each SETJ cell provide us with a wide range of flexibility to design different cellular operations. Two kinds of parameters can be used to change the dynamics of a SETJ CNN; namely, the DC biases and the pump source. In this note, we only studied the cases when the DC bias is used as an “input image”. Many more cellular operations can be implemented if we can also change the pump source.

References

- [1] L.O. Chua. *CNN: A vision of complexity*. World Scientific, Singapore : River Edge, N.J., 1998.
- [2] L.O. Chua and L. Yang. Cellular neural networks: Applications. 35(10):1273–1290, 10 1988.
- [3] L.O. Chua and L. Yang. Cellular neural networks: Theory. 35(10):1257–1272, 10 1988.
- [4] T. Ohshima and R.A. Kiehl. Operation of bistable phase-locked single-electron tunneling logic elements. *Journal of Applied Physics*, 80(2):912–923, 15 July 1996.